SIMS studies of Allende projectiles fired into Stardust-type aluminum foils at 6 km/s

Peter Hoppe[1], Frank J. Stadermann[2], Thomas Stephan[3],

Christine Floss[2], Jan Leitner[3], Kuljeet Marhas[1], and Friedrich Hörz[4]

[1]Max-Planck-Institute for Chemistry, Particle Chemistry Department, PO Box 3060, 55020 Mainz, Germany (hoppe@mpch-mainz.mpg.de)

[2]Laboratory for Space Sciences, Physics Department, CB 1105, Washington University, 1 Brookings Drive, Saint Louis, MO 63130-4862, USA (fjs@wustl.edu)

[3]Institut für Planetologie, Universität Münster, Wilhelm-Klemm-Str. 10, 48149 Münster, Germany (stephan@uni-muenster.de)

[4]NASA Johnson Space Center, Houston, Texas 77058, USA (friedrich.p.horz@nasa.gov)

ABSTRACT

We have explored the feasibility of C-, N-, and O-isotopic measurements by NanoSIMS and of elemental abundance determinations by TOF-SIMS on residues of Allende projectiles that impacted Stardust-type aluminum foils in the laboratory at 6 km/s. These investigations are part of a consortium study aimed at providing the foundation for the characterization of matter associated with micro-craters that were produced during the encounter of the Stardust space probe with comet 81P/Wild 2. Eleven experimental impact craters were studied by NanoSIMS and eighteen by TOF-SIMS. Crater sizes were between 3 and 190 µm. The NanoSIMS measurements have shown that the crater morphology has only a minor effect on spatial resolution and on instrumental mass fractionation. The achievable spatial resolution is always better than 200 nm, and C- and O-isotopic ratios can be measured with a precision of several percent at a scale of several 100 nm, the typical size of presolar grains. This clearly demonstrates that presolar matter, provided it survives the impact into the aluminum foil partly intact, is recognizable even if embedded in material of Solar System origin. TOF-SIMS studies are restricted to materials from the crater rim. The element ratios of the major rock-forming elements in the Allende projectiles are well characterized by the TOF-SIMS measurements, indicating that fractionation of those elements during impact can be expected to be negligible. This permits information on the type of impactor material to be obtained. For any more detailed assignments to specific chondrite groups, however, information on the abundances of the light elements, especially C, is crucial.

1. INTRODUCTION

Extraterrestrial matter exhibits characteristic fingerprints of elemental and isotopic compositions. At the macroscopic scale, isotopic anomalies are generally small (permil to percent level) but elemental and isotopic compositions of bulk samples can be used to differentiate between different types of meteorites. Rare, but important constituents of primitive meteorites are presolar dust grains that survived the events that led to the formation of the Solar System (Hoppe and Zinner 2000; Zinner 2004). Presolar grains are characterized by large isotopic anomalies in their major elements (e.g., C and O) compared to matter that formed in the Solar System itself, indicating that they formed around evolved stars (mainly red giants and supernovae). Presolar grains can be analyzed with high precision in the laboratory, and have provided a wealth of astrophysical information. Presolar minerals identified to date include diamonds, silicon carbide (SiC), graphite, silicon nitride (Si_3N_4), corundum (Al_2O_3), spinel ($MgAl_2O_4$), hibonite ($CaAl_{12}O_{19}$), and various silicates. Recently, presolar grains were also found in interplanetary dust particles (IDPs) (e.g., Messenger et al. 2003; Floss et al. 2004: Stadermann and Floss 2004) and in Antarctic micrometeorites (Yada et al. 2005). In many IDPs the abundances of presolar grains are higher than those in primitive meteorites, indicating the primitive nature of these particles (Messenger et al. 2003; Floss and Stadermann 2004). IDPs also exhibit widespread isotopic anomalies in H and N (enrichments in D and ^{15}N), often associated with organic matter, that are believed to be the result of chemical reactions in the cold and dense molecular cloud from which our Solar System formed (Messenger and Walker 1997).

Comets are believed to represent the most primitive matter in our Solar System. Our current understanding of the chemical and isotopic composition of comets is partly based on in-situ studies, e.g., the flyby of comet 1P/Halley in 1986 (Jessberger et al. 1988; Jessberger and Kissel 1991), partly on spectral and other remote sensing studies of cometary coma. In contrast, the ongoing Stardust mission has collected cometary material during the flyby of comet 81P/Wild 2, as well as contemporary interstellar dust (Brownlee 2003; Tsou 2003); therefore, it is the first mission to return extraterrestrial material from a specific Solar System object other than the Moon. After return of the cometary samples to Earth in January 2006, the primary goal will be to determine the elemental, isotopic, mineralogical, and organic composition of the dust.

The Stardust mission will provide two different types of capture media containing cometary samples (Tsou 2003). The primary sampling material is low-density silica aerogel. In addition to the 1039 cm^2 surface area of exposed aerogel, composed of 132 individual cells, some 153 cm^2 of aluminum foil (Al 1100; >99 % pure) was exposed. The primary purpose of this foil was to fix the aerogel in the modular collector trays and to facilitate the removal of individual tiles following return to Earth.

Although particles are not expected to survive unaltered at an encounter speed of 6.1 km/s, the Al foil represents a valuable target material, especially for small (sub-micrometer) or loosely aggregated, fluffy particles that will disintegrate during penetration of the aerogel and that cannot, therefore, be extracted with ease from this highly porous and friable capture medium. Isolated presolar grains or organic interstellar matter are expected to retain their isotopic signatures during impact and, even if they are embedded in matter of Solar System origin, it is expected that their specific isotopic fingerprints, although likely to be diluted, can still be recognized. In addition, even totally vaporized projectiles can still be identified on the basis of thin–film vapor deposits that are accessible for SIMS analyses (Stadermann et al. 1994).

Here, we report on NanoSIMS and TOF-SIMS analyses of crater residues on Al foils from impact experiments using material from the Allende CV3 meteorite. The measurements were done with the Cameca NanoSIMS 50 ion microprobes at Washington University in St. Louis and at the MPI for Chemistry in Mainz and with the ION-TOF TOF-SIMS IV instrument at the University of Münster. The NanoSIMS (Hillion et al. 1994), characterized by high spatial resolution and high sensitivity, has been successfully applied to the study of a variety of presolar materials in the past (e.g., Floss et al. 2004; Hoppe and Besmehn 2002; Messenger et al. 2003; Mostefaoui and Hoppe 2004; Nguyen and Zinner 2004; Stadermann et al. 2005). The TOF-SIMS technique has been used for the analysis of extraterrestrial matter for more than a decade (Stephan 2001) including the analysis of impact residues from LDEF (Stephan et al. 1992) and the Hubble Space Telescope solar array (Stephan et al. 1995).

In anticipation of the Stardust samples, the major goals of this study were to answer the following questions: Are isotopic measurements of crater residues feasible by NanoSIMS? What is the achievable lateral resolution and what is the precision for the measurement of the

4

isotopic compositions (C, N, O) of objects with the typical size (200 nm to >1 μm) of presolar grains? How well can the chemical composition of Allende be reproduced by the analysis with TOF-SIMS?

2. EXPERIMENTAL

Powdered bulk material of the CV3 chondrite Allende with a nominal size range of 38–43 μm was shot-gunned into Al foils at a velocity of 5.9 – 6.1 km/s using a 5 mm caliber Light Gas Gun at NASA Johnson Space Center. The foils used are flight spares from Stardust, kindly provided by Dr. P. Tsou, JPL; they are >99% pure (Al 1100 series) and 100 μm thick and they draped a massive Al back plate, akin to the foils exposed on Stardust. Earlier studies had shown that projectiles of this size are expected to produce craters as large as 180 μm (Hörz et al. 1995; see also Kearsley et al., this volume). Due to the modestly coherent nature of the Allende meterorite, substantial fragmentation of the nominal projectiles occurs during light gas gun acceleration ($> 10^6$ g) , and a wide range of fragment-associated crater sizes resulted in the present experiments. Actual projectiles responsible for many very small craters may thus be compositionally and mineralogically variable, ranging from e.g. pure Allende matrix to monomineralic grains. Also, most craters are produced by Allende projectiles, yet some craters may also be due to unavoidable gun debris, such as abrasion products of the gun barrel or debris from the burst high pressure diaphragm. Typically, on a square target some 2 cm on the side, tens of craters are being produced in a single experiment. Their diameters were shown to lie between <1 and 200 μm, with most craters measuring <2 μm. For the SIMS studies we concentrated on the larger craters with sizes between 3 and 190 μm.

Scanning electron microscopy (Leo 1530 FESEM at MPI for Chemistry and JEOL 840A SEM at Washington University), and optical scanning at the University of Münster was used to investigate the crater distribution and crater sizes on the Al foils (Figs. 1 and 2). A total of 29 craters on several Al foil pieces were selected for the SIMS analyses: NanoSIMS measurements were performed on 4 craters, 15 to 30 μm in size, at Washington University and on 7 craters (4 of which were located on an Al foil piece that was flattened prior to analysis), 3 to 30 μm in size, at MPI for Chemistry. The flattening was achieved by pressing

the Al foil between two stainless steel plates. TOF-SIMS analyses were made on 18 craters, 4 to 190 μm in size, at the University of Münster. The detailed measurement scheme is given in Table 1.

The NanoSIMS measurements followed procedures previously applied in the study of extraterrestrial matter (Floss and Stadermann 2004; Mostefaoui and Hoppe 2004). Measurements were made with a Cs^+ primary beam and parallel detection of the following negative secondary ions: $[^{16}O, {}^{17}O, {}^{18}O, {}^{28}Si, {}^{27}Al^{16}O]$ and $[^{12}C, {}^{13}C, {}^{12}C^{14}N, {}^{12}C^{15}N, {}^{28}Si]$ at MPI for Chemistry, $[^{12}C, {}^{13}C, {}^{16}O, {}^{17}O, {}^{18}O]$ at Washington University. Prior to analysis, Cs was implanted for several minutes with comparatively high primary current (~20 pA) into the region of interest to remove surface contamination and to get stable secondary ion yields. For the analysis, a primary Cs^+ ion beam of <1 pA was focused into a spot of <100 nm and raster ion images (256×256 to 1024×1024 pixels) of variable size were recorded for the selected craters. Images consist of up to 40 consecutive scans (layers) with total analysis times up to several hours per image. The measurement of isotopic standards was not necessary as the primary goal was to investigate the effects of crater topography on secondary ion signal intensity, lateral resolution, and instrumental mass fractionation for C-, N-, and O-isotopic measurements.

TOF-SIMS allows a comprehensive elemental analysis with relatively high lateral resolution and minute sample consumption (Stephan 2003). During a typical analysis, less than one atomic monolayer is consumed while the sample is rastered with a ~0.2 μm Ga^+ primary ion beam. All secondary ions of a single polarity are detected quasi simultaneously after their passage through the time-of-flight spectrometer. Both polarities are measured in two consecutive analyses. Elemental, isotopic, and molecular compositions are determined in parallel. Further details on the TOF-SIMS technique are given in the literature (Stephan 2001).

In the present study, all sample regions selected for TOF-SIMS analysis were measured after sputter cleaning by Ar ion bombardment. This cleaning was necessary since the entire Al foil was covered with a thin layer of mainly organic contaminants from the vaporized, polyethylene projectile sabot. Based on the distributions of Mg, Si, Ca, and Fe, regions of interest were selected, and complete mass spectra were generated for these regions. Mass

spectra obtained from foil areas outside the craters were used for blank correction. For this blank correction, Al/Si-ratios of the projectile material were assumed to be CV-chondritic. The surplus in Al was attributed to the target blank. Bulk element ratios were calculated using relative SIMS sensitivity factors obtained from glass standards that are usually used for quantitative TOF-SIMS analysis of silicates (Stephan 2001).

3. RESULTS AND DISCUSSION

3.1. NanoSIMS studies

The unflattened craters were investigated to determine the feasibility of direct NanoSIMS analysis of these geometrically complex structures. Since the NanoSIMS has coaxial primary and secondary ion beams that are normal to the sample surface (Fig. 3a), it should be possible to image the entire crater without direct shading from the walls. This assumption turned out to be correct (Fig. 4), although the signal intensity was in some cases significantly reduced for ions extracted from the crater bottom. The apparent reduction turned out to be the result of a secondary ion beam alignment, which was optimized for the extraction of secondary ions from the exact height of the surrounding Al foil reference level (Fig. 5). By changing the secondary ion beam focusing plane, it was in many cases possible to increase the yield of secondary ions from the crater bottom.

The surface of the Al foil shows significant contamination with a variety of elements, which interferes with an elemental or isotopic characterization of the debris material. Brief sputter cleaning with the primary beam in the SIMS instrument, however, was in most cases sufficient to remove the ubiquitous surface contamination layer. The remaining material on the surface of the Al foil is most likely residue from the impactor. The lateral resolution of the secondary ion images is important since a large fraction of previously identified presolar phases is in the sub-micrometer size range. Under ideal conditions, with a flat sample, the NanoSIMS can routinely resolve details as small as 50–100 nm. The lateral resolution in the crater bottom is somewhat reduced due to the distortion of the electrical extraction fields. However, several tests show (Figs. 6, 8, and 9) that a spatial resolution on the order of 100–

200 nm can be achieved even under less than ideal conditions. In completely flattened crater-samples, the standard lateral resolution of 50–100 nm can be achieved.

The main purpose of the NanoSIMS measurements in the initial stage of the Stardust analyses will be the isotopic characterization of impact debris associated with micro craters. It is thus important to know to what extent the determination of isotopic ratios is affected by the extreme morphometry of such craters. Si- and O-rich (Allende) material was found in all analyzed craters. Examples are shown in Figs. 5–9. Several tests clearly demonstrated (Figs. 6 and 7) that edge, slope, and sample height variations only have a minor effect on the measured isotopic ratios. For selected craters we divided the crater area into sub-areas and calculated the $^{17}O/^{16}O$ and $^{18}O/^{16}O$ ratios in all sub-areas. The standard deviations of this data set can then be used to quantify variations in instrumental mass fractionation across the craters and the limitations imposed by counting statistics. This is to test whether isotopic heterogeneities would be recognizable, should presolar grains, assumed to be embedded in material of Solar System origin, survive the foil impact partly intact. For sub-areas with sizes between 300 and 1200 nm (depending on crater size) we obtain standard deviations of 8–16 % for $^{17}O/^{16}O$ and 5–10 % for $^{18}O/^{16}O$, clearly sufficient to recognize presolar grains. These values are somewhat larger than expected from counting statistics, attesting to the fact that instrumental mass fractionation varies at the percent level across the crater. No significant difference was observed between flattened and unflattened craters. Bulk $^{17}O/^{16}O$ and $^{18}O/^{16}O$ ratios (i.e., from the integrated O signal across the whole crater) between different craters on the same Al foil were found to differ typically by 1–2 %. Since O isotopic compositions in presolar grains typically vary by a factor of 2 and sometimes even more (Messenger et al. 2003; Mostefaoui and Hoppe 2004; Nguyen and Zinner 2004; Nittler et al. 1997; Zinner et al. 2005), it will be possible to identify presolar materials among the debris particles.

C-rich grains were found in the majority of analyzed craters. One example is shown in Fig. 9. The mineralogy of the C-rich particles could not be determined. Whether they are from Allende or actual contamination is difficult to discern, but contamination seems to be more plausible. In addition, a smaller amount of C is dispersed over the whole crater. The calculated standard deviations of $^{12}C/^{13}C$ and $^{15}N/^{14}N$ ratios of the C-rich particles (150–500 nm) in Fig. 9 are 5% and 26 %, respectively. At least for C this would be sufficient to identify

8

carbonaceous presolar grains as most of these grains have isotopic anomalies of more than several tens of % (e.g., Hoppe and Zinner 2000; Zinner 2004).

3.2. TOF-SIMS studies

In contrast to the NanoSIMS, the primary ions in TOF-SIMS reach the sample surface at an angle of 45° (Fig. 3b). Therefore, major areas of the crater bottom are not accessible by the primary ion beam. As an example, Fig. 10 shows lateral element distributions in the area of craters UM #4 and UM #4.1. Secondary ion intensities on the right hand side of the crater rim are always highest since the primary ions reach the sample from the right and because oblique incidences increase the ion yield. The crater wall on the left hand side is hit almost perpendicularly, reducing the respective ion yields.

Another complication arises from the time-of-flight principle. Secondary ions from the crater bottom reach the detector slightly later than secondary ions of the same species that are released from the crater rim. Since the time scale is converted to a mass scale in TOF-SIMS this delay can lead to undesirable mass interferences: Elemental ions (typically at the low mass edge of a given nominal mass) from the crater bottom interfere with molecular ions (high mass edge of a given nominal mass) at the crater rim. In most cases therefore, only secondary ions from the crater rim were used to calculate element ratios. Their identification in the mass spectra was always unambiguous.

Crater UM #1 does not show any residual material for a proper impactor characterization. However, all other sample regions contain enough material for quantitative analysis. Quantitative results for all samples are summarized in Table 2 and Fig. 11: Element ratios normalized to Si show huge variations especially for small craters. Deposit UM #1.2 and crater UM #5 are clearly non-chondritic. Their Mg/Si-ratios are below $0.012 \times CV$ and $0.03 \times CV$, respectively, and other major elements are also more than a factor of 10 depleted compared to CV. Therefore, samples UM #1.2 and UM #5 were omitted for the calculation of geometric mean values shown in Fig. 11. These values are close to CV element ratios for most elements and fit well within the range defined by Allende chondrules (Rubin and Wasson 1987).

Since sputter cleaning was necessary prior to TOF-SIMS analysis, no useful information on organic constituents of the projectiles could be obtained. Organic compounds usually fragment during Ar bombardment. Typical silicone oil fragments as well as polycyclic aromatic hydrocarbons observed before the Ar sputtering cannot be connected with the impact craters.

Contamination of the Al foil with Li, Be, B, C, and O prevents a quantitative analysis of these elements by TOF-SIMS since secondary ion signals for these elements predominately stem from the blank. Uncertainties in the blank correction are also responsible for some of the large error bars in Fig. 11 especially for elements like Na, Si, K, Sc, and V. It is presently unknown, if this contamination is indigenous to the Al foil or if it results from the conditions during the impact experiments. Ar sputtering was not sufficient to remove this contamination completely.

Although variations in element ratios from crater to crater are rather large, the average composition of all analyzed samples resembles remarkably well the expected element pattern. If compared with element ratios of different chondrite types (Lodders and Fegley 1998), the TOF-SIMS data yield correlation coefficients above 0.92 for CV and CK, and below 0.92 for other carbonaceous chondrite classes (Table 3). On the other hand, for some ordinary and other chondrite classes, correlation coefficients above 0.92 were also found, mainly due to their low Fe and Ni concentrations. Except for CI, CH and EH chondrites, correlation coefficients are above 0.9 for all chondrite classes (Table 3). The highest correlation coefficient (0.97) was observed for geometric mean values of Allende chondrules (Rubin and Wasson 1987). Considering the size of the projectiles (~40 μm), it seems to be plausible that the projectile material mainly consists of chondrules and chondrule fragments, and that fine-grained matrix material is underrepresented. However, it should be noted that from the available data set, an unequivocal assignment to a specific chondrite class could not be made if the projectile material were unknown. For an unambiguous classification, data for light elements, especially C, would be crucial. It is hoped that the Stardust Al targets will be less contaminated and reliable data can be obtained for those elements.

4. CONCLUSIONS

The achievable lateral resolution and precision of NanoSIMS measurements of O-isotopic ratios of material inside the craters, produced at the Stardust encounter speeds, is sufficient to identify presolar matter. Larger measurement times or smaller field of views would result in an even better precision than presently observed. If presolar grains are embedded in material of Solar System origin, their recognition depends, of course, also on their survival during the impact into the Al foils. C-rich material in the Allende craters is mainly localized in hot spots and the achievable precision for $^{13}C/^{12}C$ ratios in 150–500 nm sized particles (several percent) would be sufficient to identify presolar matter among the Stardust material. For the N isotopes, longer measurement times appear desirable in order to decrease the counting statistical error on the $^{15}N/^{14}N$ ratio in N-bearing grains of the size considered here (150–500 nm); this, in principle, should be possible.

The TOF-SIMS results clearly indicate that chondritic projectiles impinging on Al foils at ~6 km/s can be identified by subsequent TOF-SIMS analysis of their residues. Element ratios of major rock-forming elements could be determined, since element fractionation during impact seems to be negligible. However, for a more detailed assignment of the projectile material to the specific chondrite classes, information on light elements is needed.

REFERENCES

Brownlee D. E., Tsou P., Anderson J. D., Hanner M. S., Newburn R. L., Sekanina Z., Clark B. C., Hörz F., Zolensky M. E., Kissel J., McDonnell J. A. M., Sandford S. A., and Tuzzolino A. J. 2003. Stardust: Comet and interstellar dust sample return mission. *Journal of Geophysical Research* 108:E8111.

Floss C. and Stadermann F. J. 2004. Isotopically primitive interplanetary dust particles of cometary origin: Evidence from nitrogen isotopic compositions (abstract #1281). 35th Lunar and Planetary Science Conference. CD-ROM.

Floss C., Stadermann F. J., Bradley J., Dai Z. R., Bajt S., and Graham G. 2004. Carbon and nitrogen isotopic anomalies in an anhydrous interplanetary dust particle. *Science* 303:1355–1358.

Hörz F., Bernhard R.P., and See T.H., 1995. Hypervelocity penetrations in aluminum 6061 and 1100 alloys. In *Shock-Wave and High Strain Rate Phenomena*, edited by Murr L.E., Staudhammer K.P., and Meyers M.A., Elsevier Science, B.V.

Hillion F., Daigne B., Girard F., Slodzian G., and Schuhmacher M. 1994. A new high performance instrument: The Cameca "Nanosims 50". In *Secondary Ion Mass Spectrometry, Proceedings SIMS IX,* edited by Benninghoven A., Nihei Y., Shimizu R., and Werner H. W. Chichester: John Wiley & Sons. pp. 254–257.

Hoppe P. and Besmehn A. 2002. Evidence for extinct vanadium-49 in presolar silicon carbide grains from supernovae. *Astrophysical Journal* 576:L69–L72.

Hoppe P. and Zinner E. 2000. Presolar dust grains from meteorites and their stellar sources. *Journal of Geophysical Research* 105:A10371–A10385.

Jessberger E. K. and Kissel J. 1991. Chemical properties of cometary dust and a note on carbon isotopes. In *Comets in the Post-Halley Era*, edited by Newburn R. L., Neugebauer M., and Rahe J. Dordrecht: Kluwer Academic Publishers. pp. 1075–1092.

Jessberger E. K., Christoforidis A., and Kissel J. 1988. Aspects of the major element composition of Halley's dust. *Nature* 332:691–695.

Kearsley A. et al., this volume.

Lodders K. and Fegley B., Jr. 1998. *The Planetary Scientist's Companion.* New York: Oxford University Press. 371 pp.

Messenger S., Keller L. P., Stadermann F. J., Walker R. M., and Zinner E. 2003. Samples of stars beyond the solar system: Silicate grains in interplanetary dust. *Science* 300:105–108.

Messenger S. and Walker R. M. 1997. Evidence for molecular cloud material in meteorites and interplanetary dust. In *Astrophysical Implications of the Laboratory Study of Presolar Materials, CP402*, edited by Bernatowicz T. J. and Zinner E. K. Woodbury, New York: AIP. pp. 545–564.

Mostefaoui S. and Hoppe P. 2004. Discovery of abundant in situ silicate and spinel grains from red giant stars in a primitive meteorite. *Astrophysical Journal* 613:L149–L152.

Nguyen A. N. and Zinner E. 2004. Discovery of ancient silicate stardust in a meteorite. *Science* 303:1496–1499.

Nittler L. R., Alexander C. M. O., Gao X., Walker R. M., and Zinner E. 1997. Stellar sapphires: The properties and origins of presolar Al_2O_3 in meteorites. *Astrophysical Journal* 483:475–495.

Rubin A. E. and Wasson J. T. 1987. Chondrules, matrix and coarse-grained chondrule rims in the Allende meteorite: Origin, interrelationships and possible precursor components. *Geochimica et Cosmochimica Acta* 51:1923–1937.

Stadermann F. J., Amari S., Foote J., Swan P., Walker R. M., and Zinner E. 1994 SIMS chemical and isotopic analysis of impact features from LDEF experiment A0187-1 and A0187-2. LDEF — 69 months in space, 3, NASA CP 3275. pp. 461–473.

Stadermann F. J., Croat T. K., Bernatowicz T. J., Amari S., Messenger S., Walker R. M., and Zinner E. 2005. Supernova graphite in the NanoSIMS: Carbon, oxygen and titanium isotopic compositions of a spherule and its TiC sub-components. *Geochimica et Cosmochimica Acta* 69:177–188.

Stadermann F. J. and Floss C. 2004. Discovery of presolar corundum (and SiC?) in an interplanetary dust particle (abstract #9045). In *Workshop on Chondrites and the Protoplanetary Disk,* LPI Contribution No. 1218, Houston: Lunar and Planetary Institute.

Stephan T. 2001. TOF-SIMS in cosmochemistry. *Planetary and Space Science* 49:859–906.

Stephan T. 2003. TOF-SIMS — a powerful tool for the analysis of stardust (abstract). In *Workshop on Cometary Dust in Astrophysics,* LPI Contribution No. 1182, Houston: Lunar and Planetary Institute. p. 71.

Stephan T., Stadermann F. J., Cramer H.-G., and Zehnpfenning J. 1992. TOF-SIMS analysis of LDEF impact residues (abstract). 23rd Lunar and Planetary Science Conference. pp. 1357–1358.

Stephan, T., Jessberger, E. K., and Bischoff, A. 1995. Hubble Space Telescope solar array microparticulate impact analysis. In *ESTEC Workshop on Space Debris on HST*, Noordwijk. 25 pp.

Tsou P., Brownlee D. E., Sandford S. A., Hörz F., and Zolensky M. E. 2003. Wild 2 and interstellar sample collection and Earth return. *Journal of Geophysical Research* 108:E8113.

Yada T., Stadermann F. J., Floss C., Zinner E., Olinger C. T., Graham G. A., Bradley J. P., Dai Z., Nakamura T., Noguchi T., and Bernas M. 2005. Discovery of abundant presolar silicates in subgroups of Antarctic micrometeorites (abstract #1227). Lunar and Planetary Science Conference. CD-ROM.

Zinner E. K. 2003. Presolar grains. In *Treatise on Geochemistry Vol I: Meteorites, Comets, and Planets*, edited by Davis A. M., Holland H. D., and Turekian K. K. Elsevier. pp. 17–39.

Zinner E., Nittler L. R., Hoppe P., Gallino R., Straniero O., and Alexander C. M. O'D. 2005. Oxygen, magnesium and chromium isotopic ratios of presolar spinel grains. *Geochimica et Cosmochimica Acta* 69:4149–4165.

Table 1. Craters in Al foils produced by Allende projectiles at some 6 km/s selected for NanoSIMS and TOF-SIMS studies.

Crater	Size (μm)	Foil preparation	Measurement	Method
WU #1	20		C, O	WU NanoSIMS
WU #2	15		C, O	**
WU #3	30		C, O	**
WU #4	20		C, O	**
MPI #1	26		C, N, O	MPI NanoSIMS
MPI #2	5		C, N, O	**
MPI #3	3		O	**
MPI #4	30	Flattening	C, N, O	**
MPI #5	13	Flattening	C, N, O	**
MPI #6	9	Flattening	O	**
MPI #7	9	Flattening	O	**
UM #1	120		Ion images + mass spectra	TOF-SIMS
UM #1.1	7		Ion images + mass spectra	**
UM #1.2	9 × 5		Ion images + mass spectra	**
UM #2	100		Ion images + mass spectra	**
UM #3	40		Ion images + mass spectra	**
UM #4	18		Ion images + mass spectra	**
UM #4.1	4		Ion images + mass spectra	**
UM #5	190		Ion images + mass spectra	**
UM #6	95		Ion images + mass spectra	**
UM #7	95		Ion images + mass spectra	**
UM #7.1	19		Ion images + mass spectra	**
UM #8	80		Ion images + mass spectra	**
UM #8.1	40		Ion images + mass spectra	**
UM #9	140		Ion images + mass spectra	**
UM #9.1	35		Ion images + mass spectra	**
UM #10	120		Ion images + mass spectra	**
UM #11	170		Ion images + mass spectra	**
UM #12	100		Ion images + mass spectra	**

Table 2. Atomic element ratios relative to Si calculated from TOF-SIMS spectra for crater residues and normalized to CV chondrites (first column according to Lodders and Fegley 1998)

	CV	#1.1	#1.2	#2	#3	#4	#4.1	#5	#6
Na	0.0265	<4.2	1.42(9)	1.5(8)	0.7(7)	0.33(7)	0.6(1)	2.416(6)	2.5(4)
Mg	1.05	1.8(1)	<0.012	1.2(1)	1.3(1)	0.522(6)	0.161(9)	0.0289(4)	1.05(3)
Si	1	1.0(7)	1.00(4)	1.0(2)	1.0(3)	1.00(3)	1.00(5)	1.000(3)	1.0(2)
K	0.00165	<8.9	0.8(2)	2(1)	2(2)	0.5(2)	1.3(3)	0.09(1)	1(1)
Ca	0.0821	0.7(1)	0.028(7)	5.7(2)	4.22(7)	0.051(5)	2.55(4)	0.272(1)	1.13(3)
Sc	0.000041	<6.7	<0.21	2(1)	1.5(9)	0.3(2)	<9.9	0.02(2)	2(1)
Ti	0.00325	<0.53	0.09(1)	1.1(5)	2.4(4)	0.15(2)	0.5(3)	0.08(2)	0.8(1)
V	0.000341	<0.67	<0.070	0.6(4)	0.8(4)	0.06(5)	<1.4	0.014(5)	0.8(3)
Cr	0.0120	1.1(1)	0.046(6)	0.66(5)	1.16(6)	0.37(1)	0.05(3)	0.0121(9)	0.31(3)
Mn	0.00495	0.9(4)	0.23(3)	0.6(1)	0.9(2)	0.66(3)	0.3(1)	0.019(2)	0.7(1)
Fe	0.753	0.84(8)	0.054(6)	0.42(6)	0.42(4)	0.413(5)	0.071(8)	0.0089(3)	0.42(2)
Co	0.00194	0.8(4)	0.02(1)	0.4(1)	0.7(2)	0.16(4)	<0.81	0.007(3)	0.4(1)
Ni	0.0402	0.4(2)	0.020(8)	0.23(6)	0.35(7)	0.13(2)	<0.082	0.013(2)	0.68(8)

	#7	#7.1	#8	#8.1	#9	#9.1	#10	#11	#12
Na	0.8(4)	1.0(4)	0.6(4)	2.6(3)	1.4(5)	0.5(1)	0.4(3)	13(1)	0.7(4)
Mg	0.90(3)	0.10(3)	1.25(3)	0.96(2)	0.92(4)	0.186(9)	1.20(2)	1.87(9)	1.11(3)
Si	1.0(2)	1.0(2)	1.0(2)	1.0(1)	1.0(2)	1.00(5)	1.0(1)	1.0(5)	1.0(2)
K	<2.4	2.6(9)	<2.2	3.5(7)	<3.2	0.5(3)	<1.8	4(3)	<2.9
Ca	2.15(3)	3.97(4)	0.49(3)	1.10(3)	1.59(4)	1.96(2)	0.77(2)	3.38(9)	1.43(3)
Sc	1.7(9)	<2.2	<2.0	<3.9	3(1)	4.7(2.4)	3(1)	5(2)	2.5(7)
Ti	0.9(2)	<0.84	0.36(9)	0.4(1)	0.8(2)	1.0(2)	0.59(9)	1.0(3)	0.8(1)
V	<0.61	<0.33	<0.83	<0.35	<0.49	0.4(3)	0.2(2)	<1.6	0.7(2)
Cr	0.53(4)	0.12(3)	0.47(5)	0.77(7)	0.76(5)	0.19(3)	0.73(3)	0.93(8)	0.79(3)
Mn	0.8(1)	0.5(1)	1.0(1)	0.6(1)	0.9(1)	0.15(6)	0.65(8)	1.1(3)	0.7(1)
Fe	0.23(2)	0.16(2)	0.40(2)	0.20(3)	0.36(3)	0.035(7)	0.39(2)	0.32(7)	0.36(2)
Co	0.2(1)	0.2(1)	<0.17	<0.34	1.0(2)	<0.31	0.6(2)	0.7(2)	0.29(7)
Ni	0.37(5)	0.26(5)	0.14(6)	0.48(9)	0.90(9)	0.13(4)	0.33(5)	0.8(1)	0.47(5)

Errors are 1σ, given as last significant digit in parentheses.

Upper limits have 2σ confidence level.

Table 3. Correlation coefficients (CC) between element ratios from crater residues and those from various chondrite types (Lodders and Fegley 1998) and Allende chondrules (Rubin and Wasson 1987).

Chondrite Type	CC	Chondrite Type	CC
CI	0.897	H	0.908
CM	0.901	L	0.955
CV	0.922	LL	0.966
CO	0.912	R	0.930
CK	0.926	Acapulcoites	0.939
CR	0.911	K	0.925
CH	0.741	EH	0.852
Allende Chon.	0.970	EL	0.936
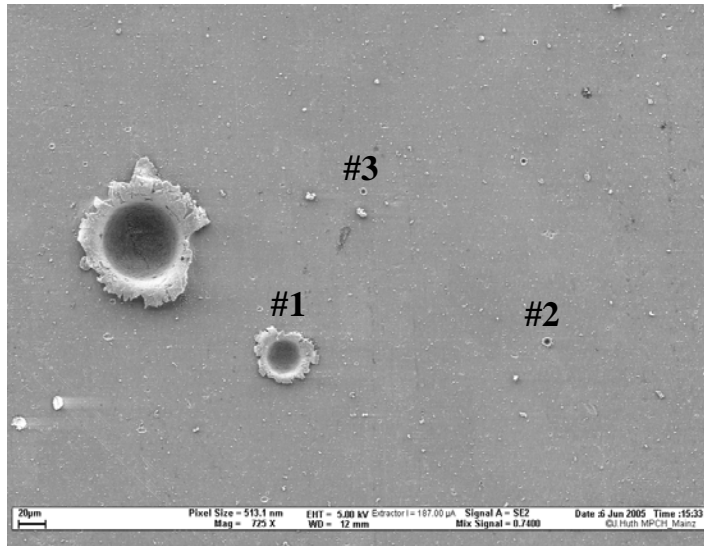
Figure 1. SEM images of three craters (MPI #1/2/3) analyzed with the NanoSIMS. Crater sizes are 16, 5, and 3 μm, respectively.
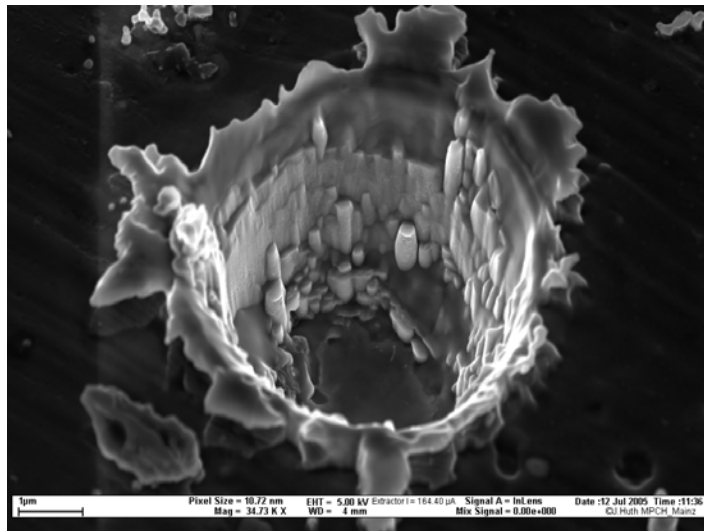
Figure 2. SEM image of crater MPI #2 after the NanoSIMS measurements. Electron detector tilted by 30 degrees. Residues of the Allende projectiles can still be recognized at the wall and on the bottom of the crater.
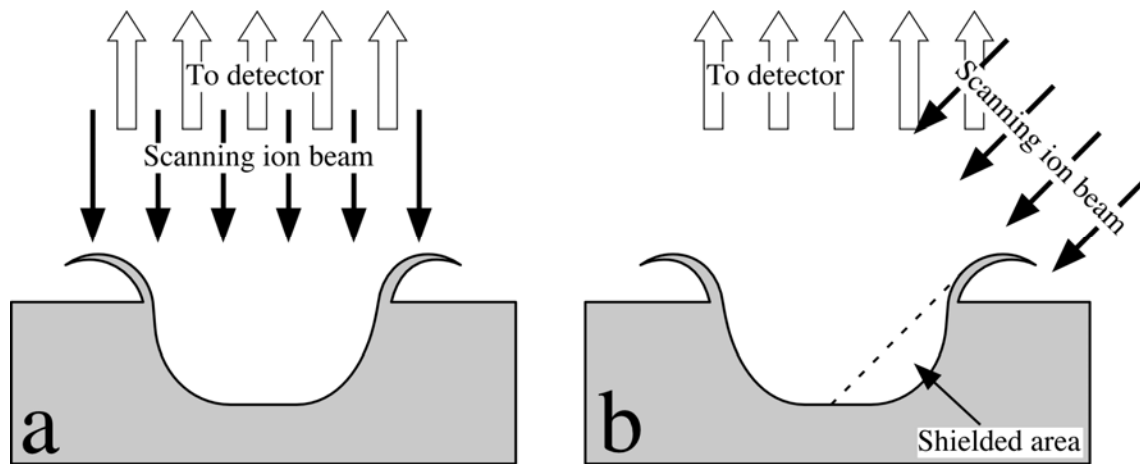
Figure 3. The ion optics of the NanoSIMS (a) are designed in such a way that both incoming primary ion beam and secondary ion extraction are normal to the sample surface. This has advantages in the analysis of (unflattened) impact craters, because the entire crater bottom is visible in most craters without direct shading from the crater walls. In contrast to this, TOF-SIMS (b) cannot analyze major parts of the crater bottom, since primary ions reach the sample surface at an angle of 45°.
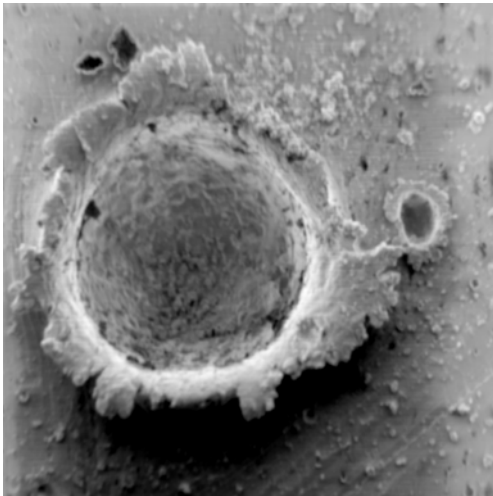
Figure 4. Aluminum foil impact as seen by NanoSIMS secondary electron (SE) imaging. The diameter of the large crater (WU #1) is 20 μm; a smaller impact crater can be seen to the right. Since secondary electrons are extracted in parallel with the secondary ions, the spatial resolution and the field of view are identical in electron and ion images, although the signal intensity is in most cases lower for secondary ions.
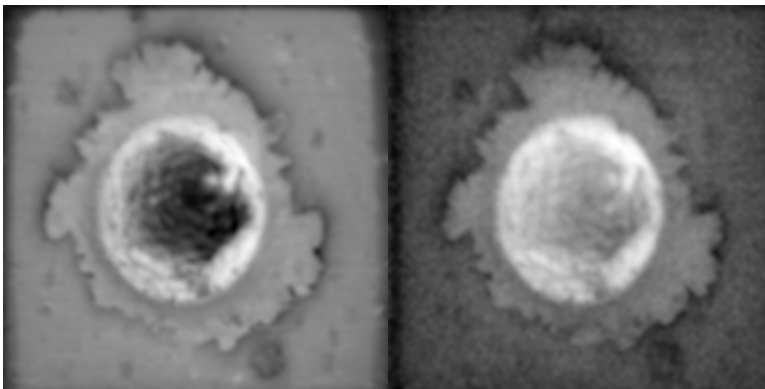

Figure 5. Two NanoSIMS images of the secondary $^{16}O^-$ signal from the same impact crater (15 μm; WU #2). The efficiency of the secondary ion extraction is sample height dependent. In the image on the left the ion extraction is optimized for the surface of the Al foil. On the right, the instrument is optimized for the extraction of secondary ions from the significantly deeper crater bottom.
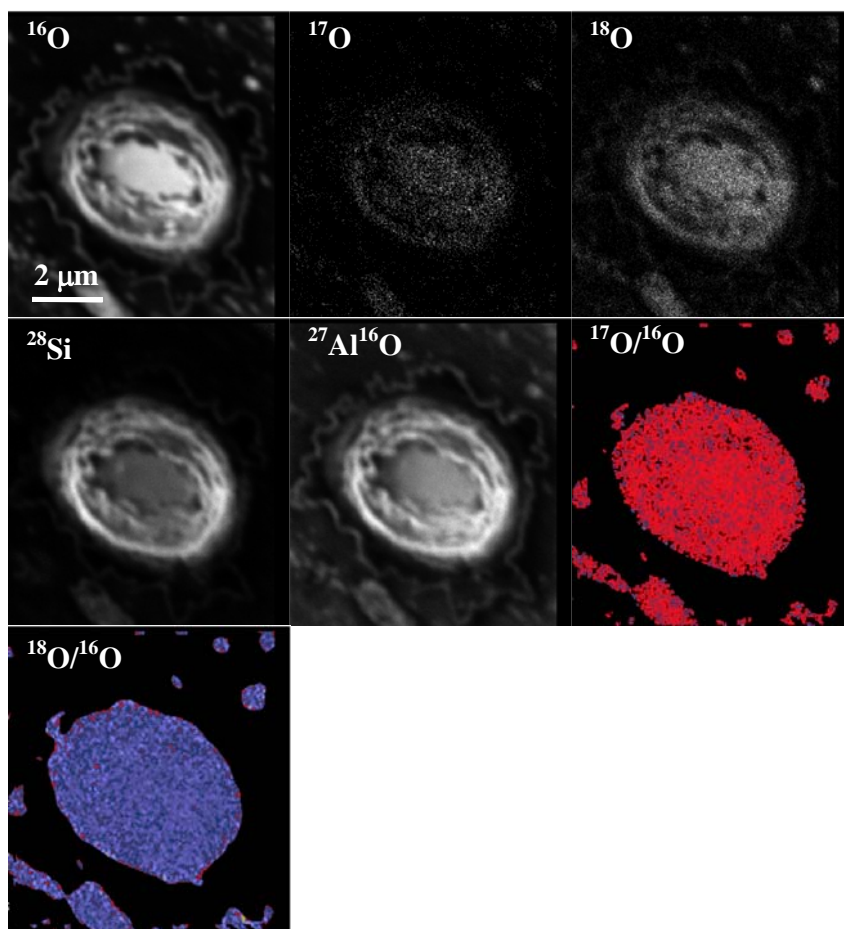
Figure 6. NanoSIMS ion images (256×256 pixel) of ^{16}O, ^{17}O, ^{18}O, ^{28}Si, and $^{27}Al^{16}O$ and false-color $^{17}O/^{16}O$ and $^{18}O/^{16}O$ ratio images of crater MPI #2. The ratio images are masked, i.e., data are only shown for those regions that have a $^{16}O^-$ intensity that exceeds 10 % of the pixel with the highest ^{16}O intensity. Standard deviations are 13 % for $^{17}O/^{16}O$ and 5.4 % for $^{18}O/^{16}O$ ratios in 12×12 pixel sub-areas (380 nm square).
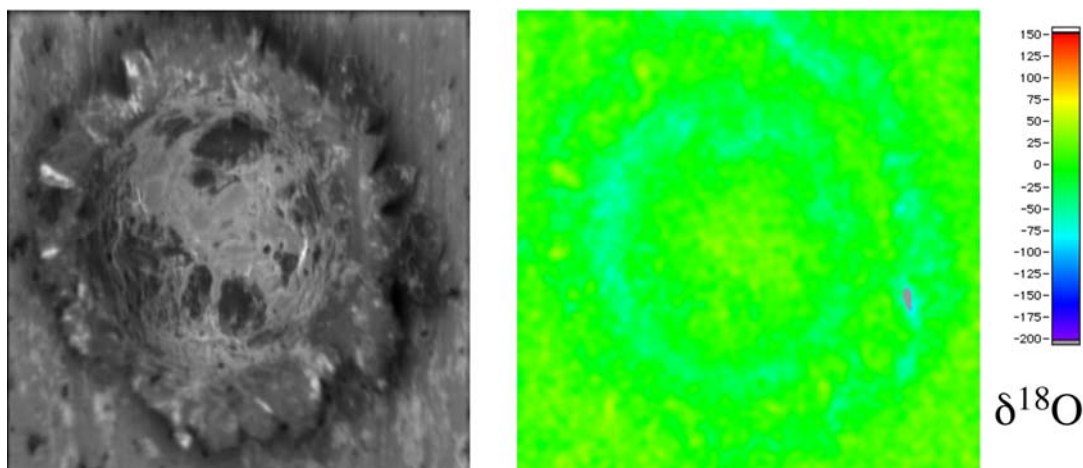
Figure 7. NanoSIMS secondary $^{16}O^-$ signal (left) and false-color $\delta^{18}O$ images (right) of an Al foil impact crater (WU #3) of 30 µm in size. Although the signal intensity varies greatly and the sample exhibits significant morphological variations, this has only a minor effect on the determination of the O-isotopic ratios.
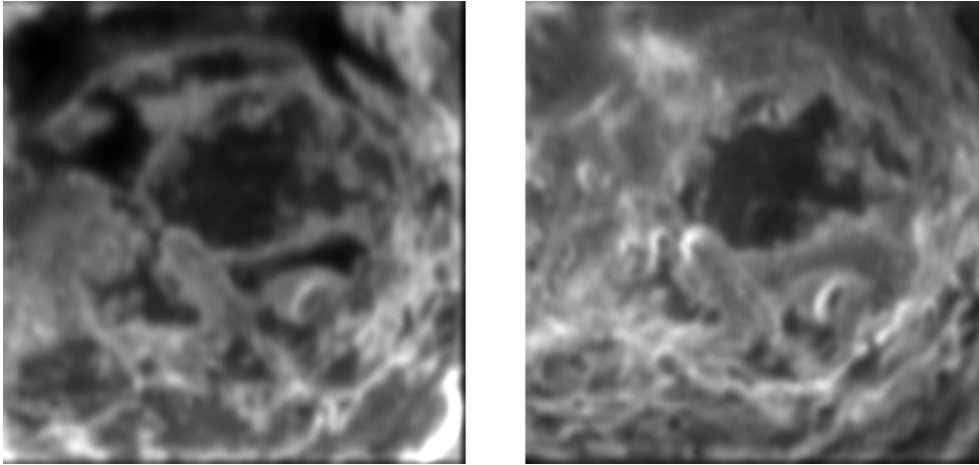
Figure 8. NanoSIMS secondary electron (SE, left) and $^{28}Si^-$ secondary ion (right) images; 10×10 µm^2 detail of the crater bottom from Fig. 7. These images demonstrate that sub-micrometer details can easily be identified in the layer of impact debris at the crater bottom.
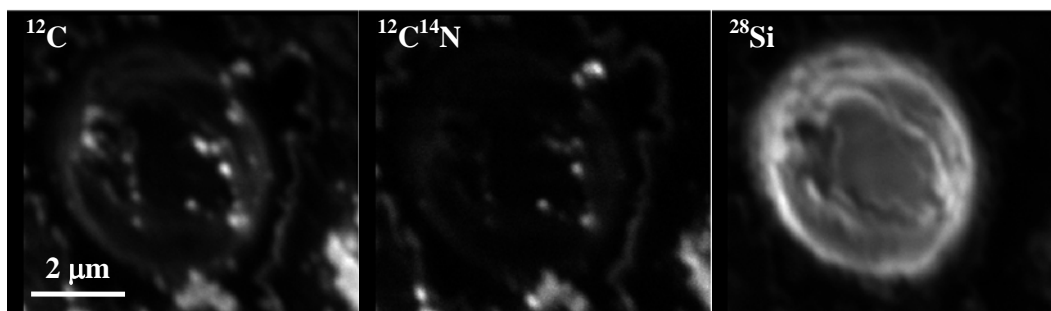
Figure 9. NanoSIMS ion images (256×256 pixel) of ^{12}C, ^{12}C^{14}N, and ^{28}Si of crater MPI #2. Small (150–500 nm) C- and N-rich particles are seen inside the crater.

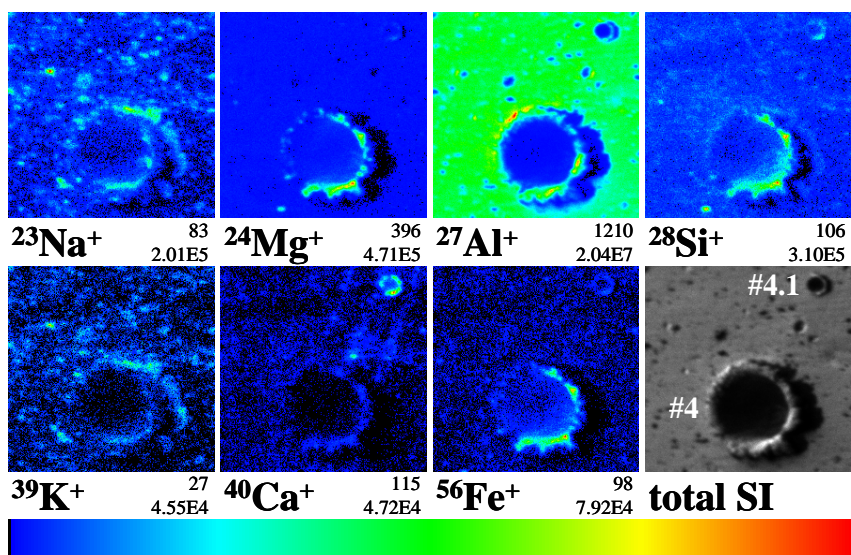|			
^{23}Na$^+$ 83 2.01E5	^{24}Mg$^+$ 396 4.71E5	^{27}Al$^+$ 1210 2.04E7	^{28}Si$^+$ 106 3.10E5
^{39}K$^+$ 27 4.55E4	^{40}Ca$^+$ 115 4.72E4	^{56}Fe$^+$ 98 7.92E4	total SI

Figure 10. TOF-SIMS secondary ion images showing two craters (UM #4 and UM #4.1) in Al foil. Field of view is 47×47 µm^2. All images use the same linear color scale normalized to the most intense pixel. Below each image, numbers for maximum and integrated intensities of the entire field of view are given. A total positive secondary ion image is given in the lower right.
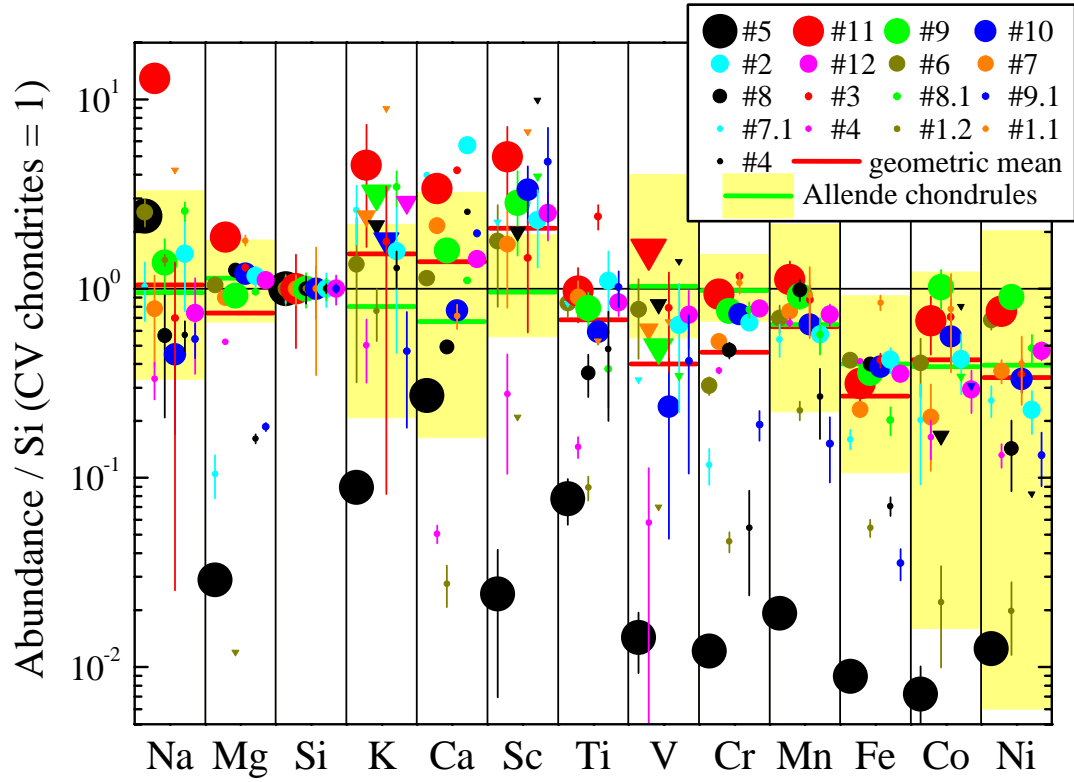
Figure 11. Element ratios, normalized to Si and CV chondrites, show huge variations. Symbol size corresponds to crater dimensions. Triangles represent upper limits. Average values were calculated using all samples except UM #1.2 and #5, which are clearly non-chondritic. Most element ratios, especially for the large craters, are within the range defined by Allende chondrules (Rubin and Wasson 1987).